Simulations of ultra-high sensitivity RI sensor in triple-core fiber with modified Vernier effect: Application in marine RI measurement*

XIONG Lingyi[1], YU Yangfei[2], DUAN Shaoxiang[1,3], LIU Bo[1,3], LIN Wei[1], and YAO Yuan[1,3]**

1. Institute of Modern Optics, Tianjin Key Laboratory of Optoelectronic Sensor and Sensing Network Technology, Nankai University, Tianjin 300350, China

2. Marine Protected Area Administration of Sansha City, Sansha 573100, China

3. Southern Marine Science and Engineering Guangdong Laboratory, Zhuhai 519000, China

(Received 4 February 2023; Revised 16 March 2023)

We proposed an ultra-high sensitivity triple-core fiber refractive index (RI) sensor with a modified Vernier effect for marine RI measurement and demonstrated it by numerical simulation. This sensor composes a pair of parallelized spatial mode Mach-Zehnder interferometers (MZIs), both of which are involved in sensing, but possess different interfering modes. By designing an MZI RI fiber optic sensor based on Vernier effect in air, it is demonstrated that in the low RI such as air environment, only the modes involved in sensing interference are affected by the environment to generate Vernier effect. In the high RI marine environment, both sensing interferometer and reference interferometer need to be affected by the ambient RI to generate Vernier effect. The simulation results indicate that the proposed novel sensing structure can amplify its sensitivity from −15 428 nm/RIU to −24 857 nm/RIU in the marine environment.

Document code: A **Article ID:** 1673-1905(2023)08-0481-6

DOI https://doi.org/10.1007/s11801-023-3020-2

The oceans cover 71% of the earth's surface and contain 99% of the living space on the earth, yet less than 10% have been explored so far[1,2]. Oceans are the main carbon sink and play an important role in regulating the global climate[3,4]. As human activities become more frequent, the marine environment is increasingly affected. Massive emissions of greenhouse gases are causing increased sea level rise and more and more extreme weather[5-7]. Ocean acidification causes mass coral bleaching and weakens the skeletons of crustaceans[8-10]. Marine pollution from human emissions, such as microplastic particles[11], heavy metals[12], red tides[13], and other serious threats are harmful to biosecurity. Therefore, more and more scientists are focusing on the research of sensing, detection, and removal of marine pollutants, especially those in marine.

Many types of sensors for marine applications have been reported in recent years. Fiber optic sensor is an excellent sensor with compact structure, high sensitivity, anti-electromagnetic interference, and corrosion resistance, which is very suitable for application in the complex marine environment[14]. In 2020, QIAN et al[15] used a large core offset splicing sensing structure to measure the temperature in marine environment with a sensitivity of 2.293 pm/°C. In 2021, CHEN et al[16] used a self-referencing optical fiber pH sensor with a precision of approximately 0.02 pH units. In 2022, LIU et al[17] used multiple-fiber Bragg grating for the measurement of depth, vibration, and temperature. However, there are still some problems with fiber optic sensors, such as insufficient sensitivity and complex structures.

In fiber optic sensors, the Vernier effect of interference superposition has the effect of sensitivity amplification[18,19]. In 2018, ZHAO et al[20] reported a relative humidity sensor based on the Vernier effect with GQDs-PVA un-fully filled in hollow-core fiber, the sensitivity changing from 19.63%RH to 78.86%RH. In 2020, LU et al[21] constructed a label-free Vernier pressure sensor by few-mode fiber, and the sensitivity is up to 4.072 nm/MPa. In 2022, HUANG et al[22] reported a high and online tunable sensitivity fiber temperature sensor based on the Vernier effect, and the sensitivity is up to −9.99 nm/°C. More and more scholars are applying the fiber optic Vernier effect in the field of gas sensing detection, but less in the field of seawater detection. This is because the refractive index (RI) of seawater is much higher than that of air, which will greatly inhibit the Vernier effect. At the same time, the currently reported fiber

* This work has been supported by the National Natural Science Foundation of China (Nos.11774181, 62231005, 62275131 and 62105164), the Natural Science Foundation of Tianjin (Nos.19JCYBJC16700, 20JCQNJC01480, 21JCQNJC00210 and 21JCYBJC00080), the Tianjin Graduate Research Innovation Project (No.2022BKY006), the Tianjin Development Program for Innovation and Entrepreneurship and the Fundamental Research Funds for the Central Universities, Nankai University.

** E-mail: l56161778@qq.com

optic Vernier sensors for the generation of multiple interference superposition, are using a complex fiber structure that has a certain production difficulty and high cost.

In this paper, a spatial pattern modulated triple-core fiber sensor for the marine environment is designed and its optimal sensing structure parameters are theoretically investigated. In the micro-SMF length of 1 200 μm, the amplification factor M of the sensor Vernier effect is about 11.5, and the sensing sensitivity is amplified from −12 828 nm/RIU to −19 343 nm/RIU. Compared with the existing marine fiber sensor, the sensing structure we designed has the advantages of high sensitivity and simple structure. We also designed a Mach-Zehnder interferometer (MZI) RI fiber optic sensor based on the Vernier effect in air, which only demonstrated the modes involved in sensing interference are affected by the environment to generate the Vernier effect. However, in the high RI marine environment, both the sensing interferometer and reference interferometer need to be affected by the ambient RI to generate the Vernier effect.

Firstly, we designed a typical MZI fiber optic Vernier sensor suitable for application in air, as shown in Fig.1. The fiber optic sensing structure consists of three common single-mode fibers (SMF) SMF-1, SMF-2, and SMF-3 fused in a staggered manner. The core diameter of SMF is 9 μm and the RI is 1.449 2. The cladding diameter is 125 μm and the RI is 1.444. The misalignment between SMF-1 and SMF-2 is 62.5 μm, with half of the core exposed. SMF-2 and SMF-3 have opposite cores, and the whole structure is symmetrically distributed.

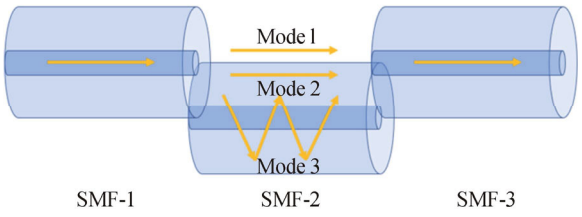

Fig.1 The structure of MZI fiber optic Vernier sensor

Due to the mismatch between SMF-1 and SMF-2, light is no longer bound in the core, but enters the air and cladding with different RIs, and a series of high-order modes will be formed, with mainly three modes shown in Fig.1.

Mode 1 is transmitted in the air inside the mismatched U-cavity, which has a fast decay rate due to the low RI of air and the influence of external environment. Mode 2 is transmitted in the SMF-2 cladding, which is less influenced by the environment, but its transmission does not satisfy the total reflection theorem and has a fast decay rate. Mode 3 is transmitted along the meridional plane in SMF-2, which is continuously reflected forward and approximately satisfies the condition of total reflection, and the intensity decay rate is low. Therefore, the effect of different mismatch lengths on the intensity number and superposition of modes is an important condition for obtaining the Vernier effect.

The spectra of the MZI fiber optic Vernier sensor with different mismatch lengths in the air were simulated and the results are shown in Fig.2. From Fig.2(a) and (b), it can be concluded that when SMF-2 approaches 700 μm, the intensity of the three modes decays to a comparable level and the Vernier effect gradually appears. When the mismatch length increases to 1 100 μm, high-order modes in SMF-2 are involved in the process of interference superposition, and the envelope pattern is no longer uniform. From Fig.2(c), it can be seen that the free spectral range (*FSR*) and contrast ratio of the Vernier envelope gradually increase with the increase of the SMF-2 length, which provides a convenient way to improve the sensitivity and sensing range. This illustrates the basic principle of generating the Vernier effect in fiber optic sensors: modulation in the fiber generates multiple spatial modes and directs the modes to interfere with each other for superposition.

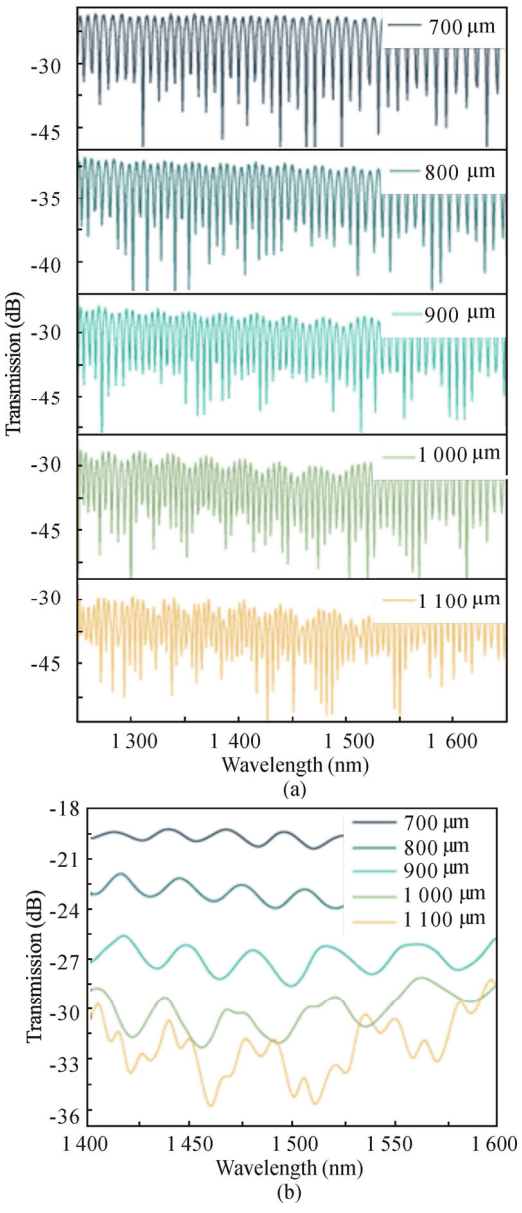

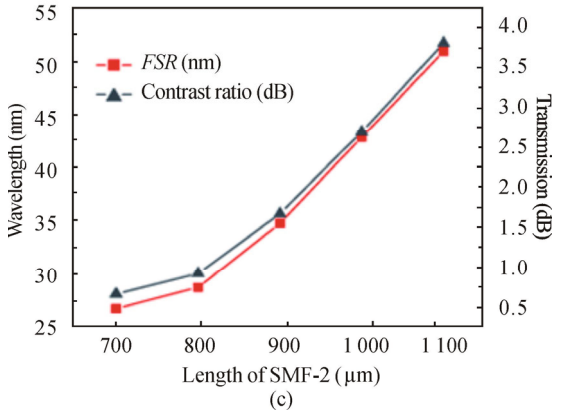

Fig.2 Influence of SMF-2 on Vernier spectra in air: (a) Transmission spectrum; (b) Spectral envelope; (c) *FSR* and contrast ratio of envelope

As shown in Fig.3(a) and (b), we calculated the spectral data of the MZI fiber optic Vernier sensor with an RI of 1.34 to simulate the marine environment, and found that the marine environment is very different from the air, and the Vernier envelope of this sensor no longer appears after entering the marine environment.

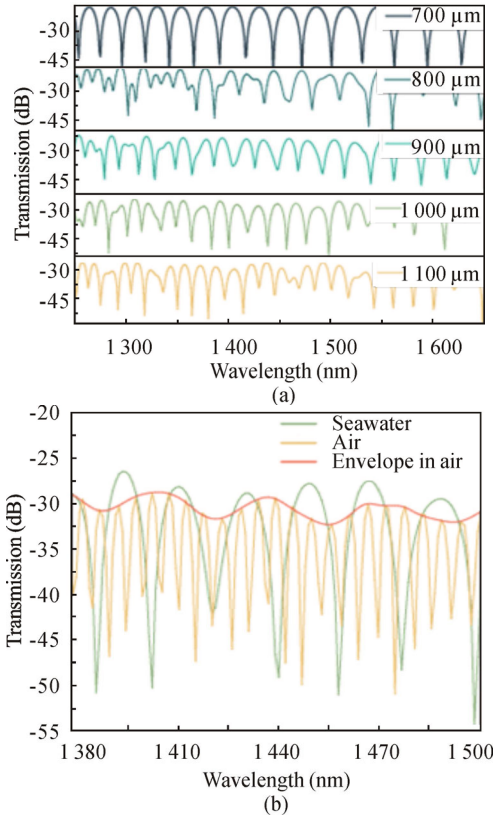

Fig.3 Spectra in marine environment: (a) Transmission spectra of different SMF-2 lengths; (b) Comparison of marine and air environment

This is analyzed because the RI inside the U-cavity has changed significantly. The RI of quartz fiber is usually at 1.44, the seawater is usually at 1.34, and the air is approximately considered as 1, so the effective RI difference inside the U-cavity is reduced from approximately 0.44 to 0.10. Effective RI difference can be expressed as

$$\Delta n_{\text{eff}} = n_{\text{fiber}} - n_{\text{environment}}. \tag{1}$$

The expression of *FSR* of the interference spectrum is as follows

$$FSR = \lambda_m - \lambda_{m+1} = \frac{\lambda_m \lambda_{m+1}}{\Delta n_{\text{eff}} L}, \tag{2}$$

where L is the optical path difference of the interference, which is represented here as the length of SMF-2. This shows that the FSR_1 formed by the interference of mode 1 and mode 2, which is called sensing interferometer, will increase significantly. As shown in Fig.3(b), FSR_1 increases from 6 nm to 18 nm. Mode 2 and mode 3 are only transmitted in SMF-2, which is less affected by the change of RI of the environment, so FSR_2 of the reference interferometer does not change much. FSR_1 will be larger than FSR_2, so we will not be able to observe the Vernier envelope. For this reason, we design a new sensing structure, its two interferometers will receive the external environmental RI perturbation, while the spatial mode regulation is more convenient, the formation of a purer spectrum, easier to obtain the Vernier effect in the marine environment, and amplify the sensing sensitivity.

We propose a new Vernier sensor, as shown in Fig.4(a). The structure consists of an SMF that introduces the light source, followed by a section of multimode fiber (MMF) fused to a length of 500 μm, which is intended to better excite the high-order modes in the fiber. Then a section of triple-core fiber, which is capable of spatial mode modulation, excites three modes that account for the dominant optical field energy, where mode 1 and mode 2 are transmitted in the U-cavity, subject to the environment. Mode 3 is transmitted in a micro-SMF with a cladding diameter of 40 μm and a core diameter of 4 μm. The micro-SMF is followed by a 500 μm MMF for mode interference and interference superposition, and the SMF is used to connect the optical signal to the spectrometer. The end-face structure is shown in Fig.4(b), where three cores are located side by side on the same diameter of the fiber, with a core diameter of 9 μm and a core-to-core distance of 31.25 μm. The core RI of triple-core fiber is 1.449 2, and the cladding RI is 1.444, the same as the MMF and micro-SMF.

From the previous analysis, it is known that the *FSR* of the interference spectrum is mainly affected by the length of the U-cavity, the same as the length of the micro-SMF. Therefore, we designed the sensors with different micro-SMF lengths and simulated the marine environment. As shown in Fig.5, it is found by the spectral analysis that as the micro-SMF length increases, the Vernier envelope gradually appears when the length reaches 900 μm.

MMF excites multiple high-order modes, and then the triple-core fiber controls the three main modes into the next sensing channel. With the limitation of MMF length,

mode 2 in the middle core has the highest energy. When entering the U-cavity part, mode 3 couples again into the micro-SMF with a finer core, the coupling efficiency is low, so the intensity of mode 3 is smaller than that of mode 1. In this sensor, the interference between mode 1 and mode 2 forms the sensing interferometer, and the interference between mode 2 and mode 3, mode 1 and mode 3 both form the reference interferometer. The interference between mode 1 and mode 3 has a similar optical path difference with the interference between mode 1 and mode 3, so the *FSR* is similar and will not affect the Vernier amplification. When the length of micro-SMF is very short, the intensity of the sensing interferometer will mask the reference interferometer, and the Vernier envelope cannot appear. When the three controllable modes decay to a comparable level, the interferometric superposition of multiple beams starts to appear as a cursor envelope.

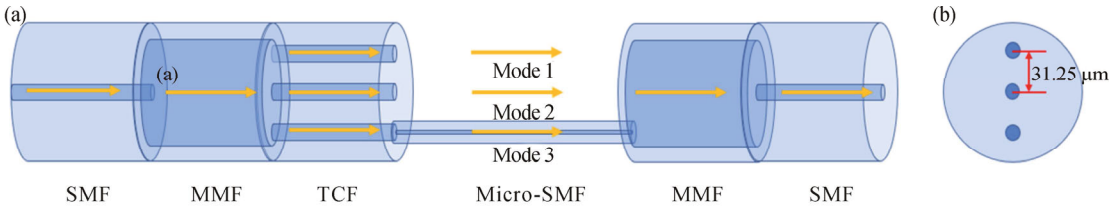

Fig.4 The new Vernier sensor: (a) Schematic diagram of the sensing structure; (b) End face of the three-core fiber

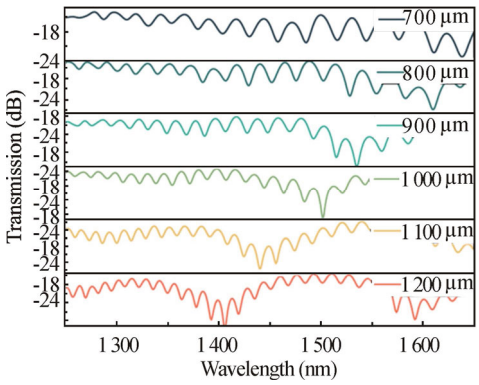

Fig.5 Effect of micro-SMF length on the Vernier sensor spectra of spatial mode modulated three-core fiber

When the length of micro-SMF increases to 1 300 μm, the intensity of mode 1 and mode 3 decays, and the sensing interferometer will be masked into the reference interferometer, and FSR_1 cannot be observed, as shown in Fig.6(a). The formula for the cursor envelope is as follows, and it is usually necessary to obtain FSR_1 and $FSR_{envelop}$ to reveal the principle of cursor sensitivity amplification. When the length of micro-SMF is 1 200 μm, the Vernier envelope is obvious, as shown in Fig.6(b).

$$FSR_{envelop}=\left|\frac{FSR_2 FSR_1}{FSR_2-FSR_1}\right|. \tag{3}$$

The sensing amplification capacity of the Vernier envelope is usually expressed in terms of the *M*-factor, and the specific expression is as follows

$$M=\frac{FSR_{envelop}}{FSR_1}=\frac{FSR_2}{FSR_2-FSR_1}. \tag{4}$$

Fig.6(c) represents the fast Fourier transformation (FFT) of the reflection spectra in Fig.6(b). The calculated *FSRs* from the sensing and reference cavities matched the spatial frequencies of the FFT spectrum. As shown in Fig.6(b), peak 1 corresponds to the sensing interferometer, and peak 2 and peak 3 correspond to the reference interferometer. Through FIR bandpass filters, we can get the sensing interference spectra and reference interference in Fig.6(d).

From Fig.6(b) and (d), we know that $FSR_{envelop}$=197 nm, FSR_1=17 nm, and the amplification *M*-factor is about 11.5 when the length of micro-SMF is 1 200 μm.

The RI of seawater is greatly affected by temperature, salinity and latitude, and is generally distributed between 1.34—1.35. In the offshore areas where human activities are frequent and detection needs are greater, the RI of seawater is usually around 1.34. The maximum sensing sensitivity can be obtained when the micro-SMF length is 1 200 μm. The transmission spectra and wavelength shift of the sensing interference are shown in Fig.7(a) and (b), and the sensing sensitivity is calculated to be −12 828 nm/RIU with a variance of 0.997 0. The variation of the Vernier envelope with the RI gradient is shown in Fig.7(c) and (d), and the sensing sensitivity is −19 343 nm/RIU with a variance of 0.969 5. This demonstrates that the Vernier envelope is useful for sensitivity amplification.

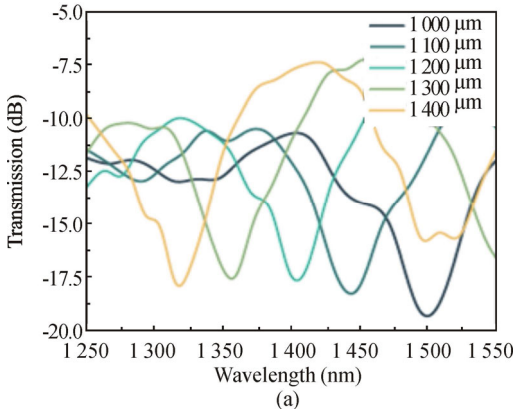

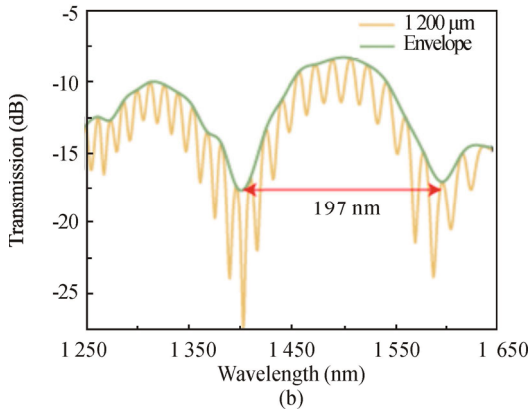

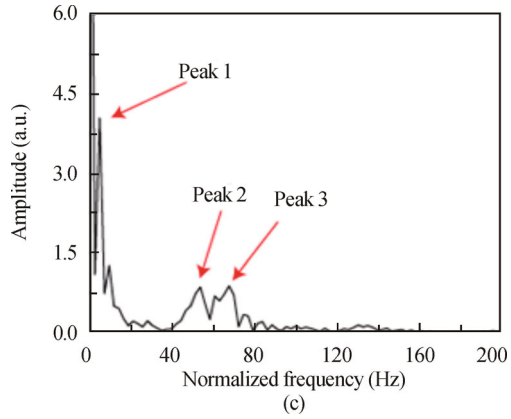

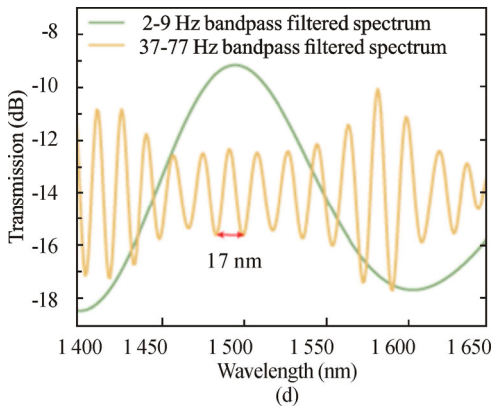

Fig.6 (a) Envelopes in different lengths of micro-SMF; (b) Spectrum and envelope diagram at 1 200 μm; (c) Fast Fourier transformation (FFT) spectrum of (b); (d) Interference spectra after FIR bandpass filters

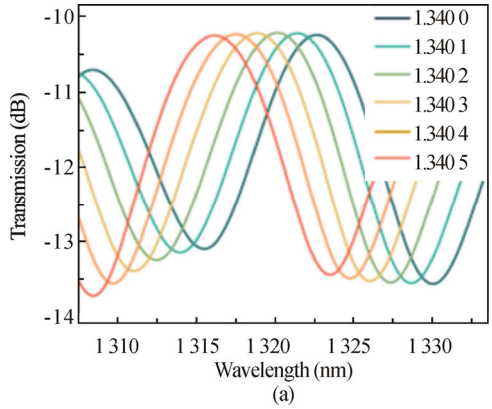

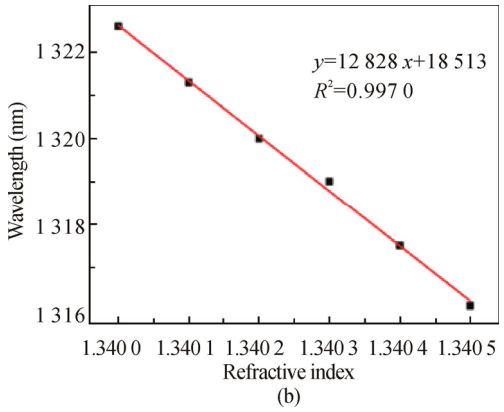

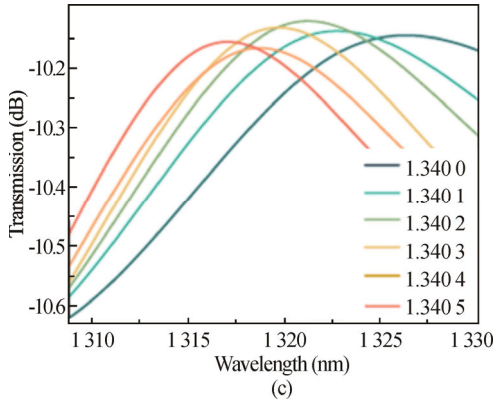

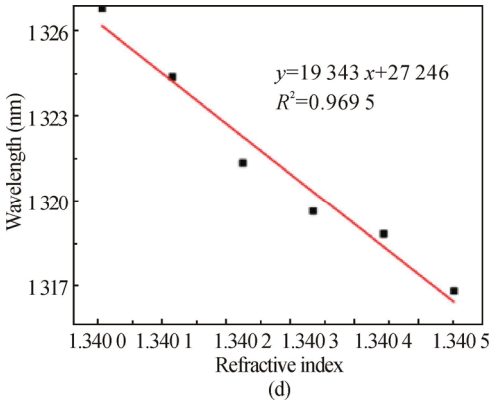

Fig.7 Transmission spectra and wavelength shift for micro-SMF length of 1 200 μm: (a) Sensing interference spectra; (b) Sensing interference wavelength drift; (c) Vernier envelope spectra; (d) Vernier envelope wavelength shift

Tab.1 Comparison between Vernier sensor and other structures in marine environment

Sensing technology	Detection target	Sensitivity
Hybrid structure MZI	Salinity	64 pm/‰[23]
Pair FBGs	Pressure	1.198 nm/MPa[24]
Large core offset interferometer	Temperature	2.293 pm/°C[25]
This work	**RI**	**-19 343 nm/RIU**

At present, fiber optic sensors used in the marine environment mainly realize the detection of physical values

such as temperature, salinity, and pressure. This is mainly because the current sensor is not sensitive, so the sensor we proposed can be applied to the detection of marine substances in the future.

In conclusion, through the design and simulation of the triple-core fiber RI sensor and MZI Vernier fiber sensor, it is found that in a low RI air environment, only sensing interference is required to be affected by the environment to achieve Vernier amplification. However, in a high RI marine environment, both sensing interference and reference interference need to be affected by the ambient RI, which increases the difficulty of sensor design. The proposed sensor realizes Vernier amplification in the marine environment through precise mode regulation, and its sensitivity increases from −12 828 nm/RIU to −19 343 nm/RIU, and its optimal structural parameters are obtained.

Ethics declarations

Conflicts of interest

The authors declare no conflict of interest.

References

[1] CHAI F, JOHNSON K S, CLAUSTRE H, et al. Monitoring ocean biogeochemistry with autonomous platforms[J]. Nature reviews earth & environment, 2020, 1(6)：315-326.

[2] RAHMSTORF S. Ocean circulation and climate during the past 120,000 years[J]. Nature, 2002, 419(6903)：207-214.

[3] HURD C L, LAW C S, BACH L T, et al. Forensic carbon accounting：Assessing the role of seaweeds for carbon sequestration[J]. Journal of phycology, 2022, 58(3)：347-363.

[4] BAUER J E, CAI W J, RAYMOND P A, et al. The changing carbon cycle of the coastal ocean[J]. Nature, 2013, 504(7478)：61-70.

[5] FRANCIS J A, VAVRUS S J. Evidence for a wavier jet stream in response to rapid Arctic warming[J]. Environmental research letters, 2015, 10(1)：014005.

[6] MORA C, SPIRANDELLI D, FRANKLIN E C, et al. Broad threat to humanity from cumulative climate hazards intensified by greenhouse gas emissions[J]. Nature climate change, 2018, 8(12)：1062.

[7] SOLOMON S, PLATTNER G K, KNUTTI R, et al. Irreversible climate change due to carbon dioxide emissions[J]. Proceedings of the National Academy of Sciences of the United States of America, 2009, 106(6)：1704-1709.

[8] HOEGH-GULDBERG O, MUMBY P J, HOOTEN A J, et al. Coral reefs under rapid climate change and ocean acidification[J]. Science, 2007, 318(5857)：1737-1742.

[9] ORR J C, FABRY V J, AUMONT O, et al. Anthropogenic ocean acidification over the twenty-first century and its impact on calcifying organisms[J]. Nature, 2005, 437(7059)：681-686.

[10] POERTNER H O, FARRELL A P. Ecology physiology and climate change[J]. Science, 2008, 322(5902)：690-692.

[11] WANG C, ZHAO J, XING B. Environmental source, fate, and toxicity of microplastics[J]. Journal of hazardous materials, 2021, 407：124357.

[12] JIN P, ZHANG J, WAN J, et al. The combined effects of ocean acidification and heavy metals on marine organisms：a meta-analysis[J]. Frontiers in marine science, 2021, 8：801889.

[13] LEE M S, PARK K A, MICHELI F. Derivation of red tide index and density using geostationary ocean color imager (GOCI) data[J]. Remote sensing, 2021, 13(298)：1-18.

[14] MIN R, LIU Z, PEREIRA L, et al. Optical fiber sensing for marine environment and marine structural health monitoring：a review[J]. Optics & laser technology, 2021, 140 (6903)：107082.

[15] QIAN J K, LV R Q, WANG S N, et al. High-sensitivity temperature sensor based on single-mode fiber for temperature-measurement application in the ocean[J]. Optical engineering, 2018, 57(10)：1.

[16] CHEN W H, DILLON W D N, ARMSTRONG E A, et al. Self-referencing optical fiber pH sensor for marine microenvironments[J]. Talanta, 2021, 225：121969.

[17] LIU Z Y, ZHANG S Q, YANG C K, et al. Submarine optical fiber sensing system for the real-time monitoring of depth, vibration, and temperature[J]. Frontiers in marine science, 2022, 9：922669.

[18] CHEN Y, ZHAO L, HAO S, et al. Advanced fiber sensors based on the Vernier effect[J]. Sensors (Basel), 2022, 22(7).

[19] GOMES A D, BARTELT H, FRAZÃO O. Optical Vernier effect：recent advances and developments[J]. Laser & photonics reviews, 2021, 15(7).

[20] ZHAO Y, TONG R J, CHEN M Q, et al. Relative humidity sensor based on Vernier effect with GQDs-PVA un-fully filled in hollow core fiber[J]. Sensors and actuators A：physical, 2019, 285：329-337.

[21] LU C, DONG X, LU L, et al. Label free all-fiber static pressure sensor based on Vernier effect with temperature compensation[J]. IEEE sensors journal, 2020, 20(9)：4726-4231.

[22] HUANG B, SHENG X, TANG Z, et al. High and online tunable sensitivity fiber temperature sensor based on Vernier-effect[J]. Optical fiber technology, 2022, 72.

[23] WANG S, LIU T, WANG X, et al. Hybrid structure Mach-Zehnder interferometer based on silica and fluorinated polyimide microfibers for temperature or salinity sensing in seawater[J]. Measurement, 2019, 135：527-536.

[24] HONGKUN Z, YONG Z, QIANG Z, et al. High sensitivity optical fiber pressure sensor based on thin-walled oval cylinder[J]. Sensors and actuators A：physical, 2020, 310：112042.

[25] QIAN J, LV R, WANG S, et al. High-sensitivity temperature sensor based on single-mode fiber for temperature-measurement application in the ocean[J]. Optical engineering, 2018, 57(10)：107101.